TECHNICAL MEMORANDUM

300

Comparison of model fluxes with surface and top-of-the-atmosphere observations

F. Chevallier and J-J. Morcrette

Research Department

January 2000

European Centre for Medium-Range Weather Forecasts
Europäisches Zentrum für mittelfristige Wettervorhersage
Centre européen pour les prévisions météorologiques à moyen

Abstract

The global observation network of the atmospheric broadband radiation reached an unprecedent extent in 1998 with the simultaneous availability of longwave and shortwave measurements of the Cloud and the Earth's radiant Energy System (CERES) instrument on board the Tropical Rainfall Measuring Mission (TRMM) spacecraft, and of a number of surface stations as part of the Atmospheric Radiation Measurement (ARM), Baseline Surface Radiation Network (BSRN) and SURFace RADiation network (SURFRAD) programmes.

In this paper, these observations are used to assess the quality of the longwave and shortwave components of both the top-of-the-atmosphere and the surface radiation budget computed by the ECMWF operational forecast system.

The main features of the boundary radiation are well captured by the system. Clouds appear to be the main modulator of the uncertainty of the top-of-the-atmosphere radiation and of the shortwave surface radiation. This is explained by both model cloud deficiencies and inadequate cloud representation in the radiative transfer schemes. The longwave surface radiation uncertainty is marked by a clear sky bias, common to most of the parametrized longwave radiative transfer models.

1 Introduction

During recent decades, the skill of weather prediction has undergone dramatic improvements. As an example, at European Centre for Medium-Range Weather Forecasts (ECMWF) the 60% level of forecast confidence has been raised from 3.5 days in 1979 to 7 days in 1997. Modellers have concentrated mainly on the validation of temperature and geopotential height, however the improvements in these quantities have increased the interest towards other variable validation: water vapour, winds, cloudiness, radiation, rain, ... This gives insight into the model deficiencies and guides corresponding improvements.

This paper uses a series of observations to focus on the radiation, both longwave and shortwave, in the ECMWF forecast system as of 1998. The characteristics of the ECMWF model are summarized in section 2. During the first seven months of 1998, longwave and shortwave flux measurements at the top of the atmosphere are available through the Cloud and the Earth's radiant Energy System (CERES) experiment, on board the Tropical Rainfall Measuring Mission (TRMM) satellite. Section 3 presents the comparisons between the CERES data and the ECMWF model outputs. At the surface, observations made as part of the Atmospheric Radiation Measurement (ARM), Baseline Surface Radiation Network (BSRN), and SURFace RADiation network (SURFRAD) programmes are available at a number of ground stations encompassing a wide range of climatic regimes from polar to tropical latitudes. Among the various observations available at each site, the present study uses the Downward Longwave Surface Radiation (DLSR) and the Downward Shortwave Surface Radiation (DSSR). The comparisons between the surface data and the ECMWF model outputs are presented in section 4. Section 5 provides an overall summary.

2 Description of the model data

The model versions used in this study are the so-called cycles 18r3 and 18r6 of the ECMWF forecast system, that were operational during 1998. The model includes a semi-lagrangian scheme together with a linear Gaussian grid (Hortal, 1999). The reduced horizontal grid corresponds to a regular grid size of about 60 *km* from the equator to the poles. In the vertical, a variable coordinate of 31 layers between the surface and the top of the atmosphere is used. The physics package is that revised at the end of 1997 (Gregory *et al.*, 1998). Of particular interest for the present study, it includes an improved version of the longwave radiative tranfer model of Morcrette (1991), with significant changes in the description of the water vapour continuum and of the ice cloud longwave optical properties. Also, a dependence of the surface longwave emissivity on the surface characteristics has been specified. The shortwave radiation transfer is based on Fouquart and Bonnel (1980), (Morcrette, 1991). The prognostic cloud scheme follows Tiedtke (1993) with some changes listed in Jakob (1994) and a revised representation of ice sedimentation.

The forecast model is initialized with the four-dimensional variational scheme described by Courtier *et al.* (1994). The assimilated observations provide information about atmospheric temperature, moisture and winds, as well as about surface characteristics.

The major change of the ECMWF forecast model during 1998 is the change of the spectral truncation from T213 to T_L319 on 1^{st} of April 1998, directly affecting the dynamical fields of winds, temperature, and surface pressure. This was accompanied by a change in the model orography.

The boundary radiative fluxes are provided by the forecast system, as values integrated over 6 hours, starting at 00, 06, 12 and 18 UTC during the first five days of forecast. The present study focusses on the archived Outgoing Longwave Radiation (OLR), Outgoing Shortwave Radiation (OSR), DLSR and DSSR. The sign convention used here makes these four radiative quantities positive. It should be noted that more than 200 model variables (temperature, water vapour, ozone, aerosols, cloud cover and cloud condensate profiles, ...) are processed by the radiative transfer schemes to produce them. Therefore, establishing the origin of their uncertainty is a mathematically ill-defined problem if the information about the input variable errors is not available. It is out of the scope of the present study to make any quantitative estimation of these. Qualitative estimations are used. Also, reference is made to previous studies.

3 Comparisons with the CERES data

3.1 Description of the CERES data

The CERES mission is part of the National Aeronautics and Space Administration's (NASA) Earth Observing System (EOS) programme. The instrument itself is an improved model of the Earth radiation Budget Experiment (ERBE) scanner instruments, which operated from 1984 through 1990 (Barkstrom, 1984). It consists of a three-channel broadband radiometer. The channels respectively measure the shortwave (0.2-5 μm), the total (0.2-100 μm) and the 8-12 μm "window" brodband radiation (Wielicki *et al.*, 1996). A set of algorithms similar to those

for ERBE has been designed to convert the measurements of these channels into broadband longwave and shortwave fluxes using spectral and angular corrections. The uncertainty of the instantaneous fluxes has been estimated to 12.7 $W.m^{-2}$ for the longwave, and to 38 $W.m^{-2}$ for the shortwave (Wielicki *et al.*, 1995). In the near future, these uncertainties are expected to be reduced with the combined use of the data from an imager flown with CERES.

Like the ERBE mission, the CERES mission has been planned to rely on a set of three satellites. The first one has been launched in November 1997 on board the TRMM spacecraft. TRMM has an orbital inclination of 35 degrees and therefore monitors the 45°N - 45°S region. Eight months worth of ERBE-like data are available, from January to August 1998. The present study makes use of the instantaneous longwave and shortwave fluxes. Due to the high volume of data, two periods of three weeks are chosen: from the 1^{st} to the 21^{st} of January, and from the 1^{st} to the 21^{st} of July. The TRMM time sampling is uneven. For the July period, most of the Southern Hemisphere as seen by the platform is in evening or in the night.

The CERES field of view is about 20 *km*. For comparison with the radiation parameters operationally provided by the ECMWF forecast system, the CERES data are averaged over the system 6-hour periods on a regular 0.5625° × 0.5625° grid, corresponding to the model TL319 resolution. For instance, during the 21-day period of July, about 3,500,000 averaged situations are available. 2,600,000 of them correspond to ocean surface conditions. According to the ECMWF 6-hour forecast, only a comparatively small number are cloud-free: about 50,000 situations, that are mostly located over land.

3.2 Results

Figure 1 presents the statistics of the differences between CERES and the ECMWF forecast model for the OLR and the OSR as a function of forecast day. The initial date runs between the 1^{st} and the 21^{st} of July. It is remarkable that the error does not grow when the atmospheric model moves away from the analysis. This may indicate that clouds play a major role in driving the error. Indeed, the ECMWF analysis system for July 1998 involves a variety of instrument observations, but none of them provides direct information about cloud cover or cloud condensate. It should be noted that some indirect information is assimilated, for instance from the radiosondes or from the Special Sensor Microwave/Imager (SSM/I). One can also notice on figure 1 that the standard deviation for the OSR significantly fluctuates with a 1-day period. This can be related to the TRMM time sampling.

Figures 2 to 5 focus on the first 6 hours of the forecast. They present the mean differences during the two 21-day periods, together with the corresponding confidence limits, given by the t statistic, and the mean CERES fields. Care must be taken in the interpretation of the maps, because of the number of error sources. Indeed three main sources may be distinguished. *The first one* lies in the atmospheric model variables, that are used as input to the radiative transfer schemes. In particular, some cloud patterns appear on the difference figures. The cloud variables that are used by the radiation schemes include the temperature, the horizontal cloud cover, the cloud condensate amount and particle size. *The second source of error* is the radiative transfer schemes, longwave and shortwave, of the atmospheric model. For instance, known deficiencies affect the way clouds are treated in the longwave (e.g., Räisänen, 1998). The distinction between the first and the second sources of error is somewhat arbitrary, because the radiative variables are part of the atmospheric model and their errors directly or indirectly

affect the other variables. Nevertheless, some atmospheric variables are better represented than the other ones in the atmospheric model, and therefore some of its errors can be directly connected with some of its parametrizations. *The third source of error* is the misinterpretation of the CERES observation system (see section 3.1). All three sources of error cumulate or compensate. In the latter case, some model weaknesses may not appear on the results, even if these ones influence the top-of-the-atmosphere radiation. In particular, the uncertainty of the CERES OSR, 38 $W.m^{-2}$, prohibits any fine examination of its discrepancies with the ECMWF model.

The difference figures are obviously correlated to cloud patterns, like those of the Inter-Tropical Convergence Zone (ITCZ) and of the South Pacific Convergence Zone (SPCZ). Thus, the OLR is very sensitive to high cloud cover. This is illustrated on figures 6a to 6c, where a weak dependence of the OLR differences is found as a function of middle and low cloud longwave emissivity, whereas a marked trend appears as a function of high cloud longwave emissivity. The OSR differences (figures 4 and 5) have larger patterns, because they are more sensitive to patterns of low and middle clouds. In particular, the stratocumulus regions off the west coast of the continents is highlighted in the shortwave difference map.

When the OLR differences are positive, like in the ITCZ over the oceans and in the SPCZ, the OSR is negative. This indicates that in these regions both the longwave and the shortwave see too much cloudiness in the atmospheric model. In July, the portion of the ITCZ over Africa appears to have a different behaviour in the model, with an insufficient northern extent as seen by the radiative transfer schemes. High positive differences exist over India and the South East Asia for the OLR in July, whereas the differences for the OSR are comparatively small. The OLR differences follow the coastlines and suggest either an overestimation of the 6-hour forecast surface temperature or a bad representation of the convection over land. In both cases, the TRMM spacecraft time sampling is likely to emphasize the discrepancies. On the contrary, high negative differences appear for the OSR North of the ITCZ over Africa in July, where there is small cloudiness. No significant differences appear for the OLR in the same region. This may indicate too low values of the atmospheric model surface albedo in July. The January maps exhibit discrepancies, for instance over the Southern hemisphere continents, the origin of which is less obvious, when comparing the OSR differences to the OLR ones. This may be due to the mixing between the different sources of errors. In particular, the model clouds may be incorrectly located both on the horizontal and on the vertical. Only the extension of the studied period, or cross-comparisons with other observations, like those of cloudiness and of surface temperature, are likely to help distinguishing between the problems.

The region covered by the TRMM spacecraft is mostly tropical. However the mean differences are likely to be higher for mid-latitude regions. Indeed figure 4b shows high differences around 40°S for the OSR in January. Symmetrical patterns (around 40°N due to the TRMM time sampling) are found in July (figure 5b). For the OLR, figure 6d shows a clear trend of the July differences as a function of the 200 hPa temperature, when the coldest 200 hPa temperatures correspond to mid-latitude air-mass types.

3.3 Discussion

The differences that are correlated with the cloud patterns are consistent with known deficiencies of the clouds in the ECMWF model. For instance, Jakob (1999) compares the 15-year

ECMWF Re-Analysis (ERA-15: Gibson *et al.*, 1997) with the International Satellite Cloud Climatology Project data (ISCCP) (Rossow and Schiffer, 1983). In particular, he shows an underestimation of the extra-tropical cloud cover over the oceans by about 10-15%, an underestimation of the stratocumulus off the west coast of the subtropical continents by 15%, and an overestimation of the cloud amount in the ITCZ, by 10-15% in the western Pacific region. All of these conclusions are coherent with the difference figures. In other respects, although the overestimation of the trade wind cumulus cover noted by Jakob (1999) on ERA-15 has been significantly reduced in the model (C. Jakob, 1999, personal communication), the shortwave errors in the corresponding regions are still large (figures 4b and 5b).

As said before, both the cloud representation in the ECMWF model and the cloud part of the radiative transfer models contribute to the discrepancies. Moreover, some of the parametrization deficiencies may partially cancel each other. As an example, the introduction of a distinction between cloud cover and cloud emissivity in the longwave radiative transfer model (Räisänen, 1998) increases the differences with CERES in the ITCZ (not shown) even though it improves the stand-alone computations. As a consequence, the various model parametrizations are developed in parallel so that their interactions are taken into account (Gregory *et al.*, 1998).

4 Comparisons with surface observations

4.1 Description of the observations

Surface radiation comparisons are made using data from 15 ground stations, which characteristics are given in table 1. Each station is part of either the ARM, the BSRN or the SURFRAD networks, and was operational during 1998. The three networks aim at providing high-quality long-term measurements of the components of the surface radiation budget. ARM and BSRN are respectively presented by Stokes and Schwartz (1994) and Ohmura *et al.* (1998). SURFRAD is dedicated to the study of the radiation over the United States (U. S.) and is a collaborative effort among the National Oceanic and Atmospheric Administration (NOAA), the National Aeronautic and Space Agency (NASA) and the U. S. university scientists.

A number of atmospheric measurements is available on each site. The present study makes use of the DLSR and DSSR observations performed by upward looking pyrgeometers and pyranometers respectively. For these quantities, all stations have adopted the standards for measurements set by BSRN (WCRP, 1991; Heimo *et al.*, 1993). These are 15 $W.m^{-2}$ for broadband solar measurements and 10 $W.m^{-2}$ for thermal infrared instruments. To achieve these goals, both the broadband solar and infrared instruments are calibrated against standards traceable to the World Radiation Centre in Davos, Switzerland. The absolute calibration is such that 90% of the measurements are within 11 $W.m^{-2}$, and 99% are within 15 $W.m^{-2}$ of the standards.

The observations are usually available with a frequency of at least 3 minutes. As for the CERES data, the broadband fluxes are averaged here over 6-hour periods for comparisons with the radiation parameters operationally provided by the ECMWF forecast system.

4.2 Results

The correlations between the 6-hour forecast surface radiation and the observations are shown in table 2 for each station. They are usually higher than 0.80 for the DLSR, even reaching 0.95 (Billings). This indicates a good representation of the variability of the low cloud cover in the model. On the other hand, poor correlations are found over Payerne (0.76), Tateno (0.73), Kwajalein (0.70), Florianopolis (0.68), and South Pole (0.76). The correlations for the DSSR (table 2, middle) are around 0.90, but the diurnal cycle greatly contributes to this result. Therefore, the statistics with only the situations which local time lies between 8 and 18 hours are presented in the right part of table 2. In this case, the correlations are rather similar to those of the DLSR, which is expected since, after the diurnal cycle, the clouds are the main modulators of both the DLSR and the DSSR.

Figures 7 and 8 present the statistics of the differences between the surface observations and the ECMWF forecast model as a function of forecast day. Distinction is made between the winter months (January and February 1998) and the summer months (July and August 1998). The seven U. S. stations are gathered together, as well as the two European stations. The two subtropical islands (Bermuda and Tateno) are also gathered together for the DLSR. Because of their different longitudes, only Bermuda is shown for the DSSR.

For the DLSR (figure 7), the standard deviations grow for most of the stations from about 20 $W.m^{-2}$ at the initial time to about 30 $W.m^{-2}$ at the fifth day. Even if its amplitude varies with the location and the season, a negative bias of about 20 $W.m^{-2}$ appears for the mid-latitude stations: those of the U. S. and those over Europe. This bias appears for each one of these stations separately considered (not shown). It exhibits a clear daily cycle without any significant trend. In particular, the morning bias is significantly reduced compared to the three other day times. A similar behaviour is seen for Florianopolis and Tateno, but in this case the morning bias is positive. The polar statistics show a strong negative bias, with no diurnal cycle as expected from these regions. The tropical islands have nearly no bias. Figures 9a to 9c show the dependence of the difference between the 6-hour forecast DLSR and the observations as a function of low, middle and high cloud longwave emissivity for the non-polar stations. It is seen that the more cloudiness there is in the model, the more reduced the bias is.

The DSSR statistics (figure 8) show strong diurnal, seasonal and latitudinal variations, as expected from the corresponding variations of the insolation. The standard deviations do not have any significant trend, and are usually more than 150 $W.m^{-2}$ in the middle of the day. The biases are mostly positive, except for the European stations and the tropical islands. The dependence of the difference between the 6-hour forecast DLSR and the observations as a function of cloudiness is presented on figure 10. The chosen cloudiness variable is the mean transmittivity in the 0.25-0.69 μm spectral region, for low, middle and high clouds. Unlike the results for the DLSR, the smaller biases and standard deviations are found for the clearest situations, as diagnosed by the forecast model. This is discussed in the next section.

4.3 Discussion

The analysis of the differences between the model values and the surface observations are still more delicate than for the comparisons with satellite measurements. Indeed, the low number of operating stations makes it difficult to link the discrepancies to the patterns of the

general circulation, as is done with CERES. Moreover, because of the model finite horizontal resolution, connected with corresponding averaged orography and land/sea repartition, some inconsistencies necessarily exist between the surface observations and the model fields. However, the results show two features common with previous validations of general circulation models: an overall overestimation of the DSSR and an overall underestimation of the DLSR (e.g., Wild *et al.*, 1995; Garratt and Pratta, 1996). Several explanations have been put forward to explain these tendencies: a possible inadequate representation of the temperature and humidity profiles in the boundary layer, as well as a deficient description of the "continuum absorption" (i.e. water vapour continuum and aerosols).

Wild *et al.* (1998) document the characteristics of the ECMWF shortwave radiative transfer model. The authors show that the clear-sky shortwave radiation at the surface is realistically captured by the radiative transfer model, even though the water vapour molecular absorption may be underestimated (Wild and Liepert, 1998). Also, Wild (1999) points at some weaknesses of the aerosol description in the tropics. This confirms the results of figure 10, where the better results are found in clear situations as diagnosed by the forecast model. The cloud absorption might be underestimated in general circulation models parametrizations (Cess *et al.*, 1995). However, Wild *et al.* (1998) show that it is partially compensated in the ECMWF shortwave scheme by the effect of the coarse spectral resolution of the code. In addition to the deficiencies of the model cloud variables (Jakob, 1999), this makes the cloudy sky results difficult to analyse.

For the DLSR, figure 9 suggests that either the observed bias mainly corresponds to clear-sky radiation, or that the radiation scheme significantly underestimates the cloudiness effects when the forecast model predicts only few cloudiness, or that these two problems are combined. Once more (see section 3.2), the radiative cloud effects stem from various origins: the cloud cover, the liquid and ice water contents, the layer overlap and the particle size of the cloud condensate. In order to assess the accuracy of the clear sky computations, a complementary experiment is performed with the data from Billings. Five days worth of data are used from 13/12/97 to 17/12/97, during which both the forecast model and the station ceilometer agree about the absence of cloudiness. The ECMWF system during December 1997 is similar to that one in January 1998. A special processing is applied during the forecast, so that the model variables are archived at each one of its time steps at the Billings grid point (the so-called DDH archives). Figure 11 shows that the forecast model tends to underestimate the DLSR by about 15 W/m^2 at most times. During the last three days of the pentad, radiosonde reports are available. Their very good agreement with a microwave estimation of the total water vapour content (less than 1.0 kg/m^2 difference) makes them reliable. Together with the ECMWF longwave radiative scheme, they are used here to make a third estimate of the DLSR, also plotted on figure 11. It is shown that the radiosonde-derived DLSR still underestimate the observed DLSR by more than 8 W/m^2. A comparable bias (12 W/m^2) is found with the Payerne data in the same conditions of experiment (M. Wild, personal communication, 1999). The use of a more accurate radiative transfer model (Mlawer *et al.*, 1997) reduces the bias of the radiosonde-derived DLSR at Billings by less than 2 W/m^2 (not shown). Results are also quite insensitive to higher vertical resolutions for the radiative computations, or to improved angular integration. The radiosonde-derived DLSR bias is not surprising. Indeed, a weak dependence of the DLSR comparisons was found as a function of the forecast day (figure 7), whereas the ECMWF system assimilates radiosonde observations at a short distance of each radiation station used here.

To explain the DLSR bias, two possible sources of error would have to be analysed. The first

one is the aerosol climatology, used as input to the radiative transfer model. Its effect should be however limited in the longwave spectrum. The second one is the water vapour continuum in the 0-500 cm^{-1} spectral band which validation has not been as extensive as for the other wave numbers, due to the lack of measurements at atmospheric temperatures (e.g., Clough *et al.*, 1989; Ma and Tipping, 1992).

An important feature of the DLSR bias is its diurnal cycle at most locations (figure 7). Figure 12 focusses on the Carpentras site. The diurnal cycles of the observed DLSR, of the model DLSR, and of the mean longwave middle cloud emissivity are shown. The maximum of cloudiness is seen in the afternoon. A possible interpretation of the figure distinguishes between two sources of bias: the clear sky bias, which mostly affects the night time, and a possible lack of afternoon cloudiness in the forecast. In this case, the optimal time for the DLSR estimation would be in the morning, as on figure 7, when both problems are reduced. This hypothesis needs to be confirmed with correspondent validation of the cloudiness diurnal cycle in the forecast model (e.g., Arpe, 1999).

5 Summary and prospects

The present study compares the boundary fluxes computed by the ECMWF forecast system in 1998 and corresponding observations from the TRMM spacecraft (CERES programme) and from surface stations (ARM, BSRN and SURFRAD programmes). The measured data, although available only after long delays, are particularly interesting for checking the model radiation, as they are obtained with the highest available accuracy for the corresponding quantities. In particular, compared to other sources of observation whose cover may be more global, they are less, or not, dependent on existing radiative transfer models.

The top-of-the-atmosphere comparisons cover the 45°S-45°N region. The discrepancies between the model and the observations are mostly correlated with cloud (ITCZ, SPCZ, stratocumulus) and surface (temperature and albedo) patterns. If the differences related to clouds are attributed to the simulated cloud variables, the results corroborate known deficiencies of the ECMWF simulated cloudiness. However, both the longwave and the shortwave ECMWF schemes, like most of the existing parametrized schemes, do not properly handle clouds. Both problems add or compensate. Because most of the top-of-the-atmosphere error of the ECMWF model are linked with cloudiness and that no cloud parameter is assimilated, the error remains stable from the first step of the forecast to at least the fifth day.

Only few meteorological stations observe the broadband components of the surface radiation. The comparisons with the model data at 15 available stations show that a high part of the flux variance (usually more than 80%) is well captured by the system. This corroborates recent encouraging results regarding the validation of the cloud distribution in the ECMWF model (e.g., Miller *et al.*, 1998). However, the quantitative analysis of the radiation comparisons indicates an overall overestimation of the DSSR by the system and an overall underestimation of the DLSR. The DLSR bias is attributed mainly to the clear-sky component, whereas the DSSR bias mostly concerns the cloud contribution to the flux. In both cases, the radiative transfer scheme strongly contribute to the error. These deficencies are common to most of the existing general circulation models and their respective origins are not understood yet. In other respects, the model flux biases have a strong diurnal cycle, that appears to stem from

both radiative transfer and atmospheric model weaknesses. This could not be shown on the previous comparisons between model surface fluxes and observations, because those focussed on monthly means only.

1998 was the last year of the 31-level ECMWF system. It was successively replaced in 1999 by 50-level and 60-level versions, with an increased vertical resolution in both the stratosphere and the boundary layer, and important changes of the model physics. On-going investigations are assessing the impact of these changes on the results presented here. In particular, a similar validation will be performed on the forthcoming ECMWF 40-year re-analysis (ERA-40).

Acknowledgments

Authors wish to thank C. Jakob for fruitful comments on the results presented here, and M. Miller for his careful review of the manuscript. The continuous help of D. Lucas in dealing with the various observation file formats was greatly appreciated.

References

Arpe, K., 1999: Differences in the hydrological cycles from different reanalyses - which one can we believe? In *Second International Conference on reanalyses, 23-27 August 1999, Wokefield Park, reading, UK*, in press.

Barkstrom, B. R., 1984 : The Earth Radiation Budget Experiment (ERBE). *Bull. Amer. Meteo. Soc.*, **65:11**, 1170-1185.

Cess and coauthors, 1995: Absorption of solar radiation by clouds: observations versus models. *Science*, **267**, 496-499.

Clough, S. A., F. X. Kneizys, and R. Davies, 1989: Line shape and the water vapor continuum. *Atmos. Res.*, **23**, 229-241.

Courtier, P., J.-N. Thépaut, and A. Hollingsworth, 1994: A strategy, for operational implementation of 4D-Var, using an incremental approach. *Q. J. Roy. Meteor. Soc.*, **120**, 1367-1388.

Fouquart, Y. and B. Bonnel, 1980: Computation of solar heating of the Earth's atmosphere: a new parameterization. *Beitr. Phys. Atmosph.*, **53**, 35-62.

Garratt, J. R., and A. J. Pratta, 1996: Downwelling longwave fluxes at continental surfaces - A comparison of observations with GCM simulations and implications for the global land-surface radiation budget. *J. Climate*, **9**, 646-655.

Gibson, J. K., P. Kållberg, S. Uppala, A. Hernandez, A. Nomura, and E. Serrano, 1997: ECMWF Re-analysis. 1. ERA description. ECMWF Project Report Series.

Gregory, D., J.-J. Morcrette, C. Jakob, and A. Beljaars, 1998: Introduction of revised radiation, convection, cloud and vertical diffusion schemes into Cy18r3 of the ECMWF integrated forecasting system. ECMWF Technical Memorandum No. 254 [available from ECMWF, Shinfield Park, Reading, Berks. RG2 9AX, UK].

Heimo, A., A. Vernez, and P. Wasserfallen, 1993: Baseline Surface Radiation Network (BSRN). Concept and implementation of a BSRN station. WMO/TD No. 579, WCRP/WMO, Geneva.

Hortal, M., 1999: The development and testing of a new two-time-level semi-Lagrangian scheme (SETTLS) in the ECMWF forecast model. *Q. J. Roy. Meteor. Soc.*, submitted.

Jakob, C., 1994: The impact of the new cloud scheme on ECMWF's Integrated Forecasting System (IFS). In *ECMWF/ GEWEX Workshop on Modelling, Validation and Assimilation of Clouds*, Reading, United Kingdom, ECMWF.

Ma, Q., and R. H. Tipping, 1991: A far wing line shape theory and its application to the water vapour continuum absorption in the infrared region. I. *J. Chem. Phys.*, **95**, 6290-6301.

Miller, S. D., G. L. Stephens, and A. C. M. Beljaars, 1998: A validation of the ECMWF prognostic cloud scheme using LITE. *Geophys. Res. Lett.*, in press.

Mlawer, E. J., S. J. Taubman, P. D. Brown, M. J. Iacono, and S. A. Clough, 1997: Radiative transfer for inhomogeneous atmospheres : RRTM, a validated correlated-k model for the longwave. *J. Geophys. Res.*, **102**, 16663-16682.

Morcrette, J. J., 1991 : Radiation and Cloud Radiative Properties in the European Centre for Medium Range Weather Forecasts forecasting system. *J. Geophys. Res.*, **96:D5**, 9121-9132.

Ohmura, A., E. G. Dutton, B. Forgan, C. Fröhlich, H. Gilgen, H. Hegner, A. Heimo, G. König-Langlo, B. McArthur, G. Müller, R. Philipona, R. Pinker, C. H. Whitlock, K. Dehne, M. Wild, 1998: Baseline Surface Radiation Network (BSRN/WCRP): new precision radiometry for climate research. *Bull. Amer. Meteo. Soc.*, **79**, 2115-2136.

Räisänen, P., 1998: Effective longwave cloud fraction and maximum-random overlap clouds - a problem and a solution. *Mon. Wea. Rev.*, **126**, 3336-3340.

Rossow, W. B., and R. A. Schiffer, 1983: The International Satellite Cloud Climatology Project (ISCCP): the first project of the World Climate Research Program. *Bull. Amer. Meteo. Soc.*, **64**, 779-784.

Stockes, G. M., and S. E. Schwartz, 1994: The Atmospheric Radiation Measurement (ARM) Program: programmatic background and design of the cloud and radiation testbed. *Bull. Amer. Meteo. Soc.*, **75**, 1201-1221.

Tiedtke, M., 1993: Representation of clouds in large-scale models. *Mon. Wea. rev.*, **121**, 3040-3061.

WCRP-54, 1991: Radiation and Climate: workshop on the implementation of the Baseline Surface Radiation Network. Washington, DC, 3-5 December 1995. WCRP Report No. 406, World Meteorological Organization, Switzerland.

Wielicki, B. A., R. D. Cess, M. D. King, D. A. Randall, and E. F. Harrison, 1995: Mission to Planet Earth : role of clouds and radiation in climate. *Bull. Amer. Meteo. Soc.*, **76:11**, 2125-2153.

Wielicki, B. A., B. R. Barkstrom, E. F. Harrison, R. R. Lee, G. L. Smith, and J. E. Cooper, 1996: Clouds and the Earth's Radiant Energy System (CERES): An Earth observing system experiment. *Bull. Amer. Meteo. Soc.*, **77:5**, 853-868.

Wild, M., 1999: Discrepancies between model-calculated and observed shortwave atmospheric absorption in Equatorial Africa. *J. Geophys. Res.*, in press.

Wild, M., and B. Liepert, 1998: Excessive transmission of solar radiation through the cloud-free atmosphere. *Geophys. Res. Lett.*, **25**, 2165-2168.

Wild, M., A. Ohmura, H. Gilgen, E. Roeckner, M. Giorgetta, J.-J. Morcrette, 1998: The disposition of radiative energy in the global climate system: GCM-calculated versus observational estimates. Climate Dynamics, **14**, 853-869.

Zhong, W., and J. D. Haigh, 1995: Improved broadband emissivity parameterization for water vapor cooling rate calculations. *J. Atmos. Sci.*, **52:1**, 124-138.

Station	Latitude	Longitude	Network
Barrow, AL, U.S.A.	71.2 N	156.8 W	BSRN/ARM
FortPeck, MT, U.S.A.	48.3 N	105.1 W	SURFRAD
Payerne, Switzerland	46.8 N	6.9 E	BSRN
Carpentras, France	44.0 N	5.0 E	BSRN
TableMountain, CO, U.S.A.	40.1 N	105.2 W	SURFRAD
Bondville, IL, U.S.A.	40.0 N	88.3 W	SURFRAD
Boulder, CO, U.S.A.	40.0 N	105.2 W	SURFRAD
Desert Rock, NV, U.S.A.	36.6 N	116.0 W	SURFRAD
Billings, OK, U.S.A.	36.3 N	97.3 W	ARM
Tateno, Japan	36.0 N	140.0 E	BSRN
GoodwinCreek, MS, U.S.A.	34.3 N	89.5 W	SURFRAD
Bermuda	32.3 N	64.7 W	BSRN
Kwajalein	8.7 N	167.7 E	BSRN
Florianopolis, Brazil	27.5 S	48.5 W	BSRN
SouthPole	89.9 S	24.4 W	BSRN

Table 1: Latitude, longitude (in degrees) and observation network of the radiation stations used in this study.

	DLSR			DSSR					
				Obs. > 0			8-16 LT		
Station	N	(N_c)	correl.	N	(N_c)	correl.	N	(N_c)	correl.
Barrow	1455	(137)	0.90	1022	(64)	0.94	298	(26)	0.92
FortPeck	1454	(360)	0.92	921	(214)	0.92	724	(159)	0.90
Payerne	1453	(231)	0.76	256	(54)	0.70	256	(54)	0.70
Carpentras	1439	(398)	0.91	1077	(322)	0.96	718	(198)	0.93
TableMountain	1457	(355)	0.85	920	(189)	0.90	727	(134)	0.84
Bondville	1458	(322)	0.95	932	(193)	0.91	728	(135)	0.86
Boulder	1433	(342)	0.88	1103	(241)	0.94	717	(128)	0.87
Desert Rock	1162	(586)	0.90	811	(384)	0.97	289	(121)	0.90
Billings	1339	(491)	0.95	835	(293)	0.89	663	(216)	0.85
Tateno	1120	(158)	0.73	338	(45)	0.84	292	(32)	0.76
GoodwinCreek	1456	(404)	0.94	845	(221)	0.89	726	(175)	0.83
Bermuda	1452	(64)	0.83	1132	(53)	0.92	364	(16)	0.72
Kwajalein	1457	(7)	0.70	1089	(6)	0.88	728	(5)	0.67
Florianopolis	1373	(49)	0.68	751	(16)	0.87	341	(7)	0.66
SouthPole	1417	(235)	0.76	738	(150)	0.95	185	(39)	0.94

Table 2: Correlation between the surface longwave and shortwave radiations in the ECMWF 6-hour forecast and the surface observations. For the shortwave radiation, distinction is made between the results taking only the situations into account where the observed DSSR is greater than 0 W/m^2, and those taking only the points between 8 and 16 local time (LT) into account. The number of available 6-hour observations (N), as well as the number of them which total cloudiness is less than 0.02 (N_c) is indicated.

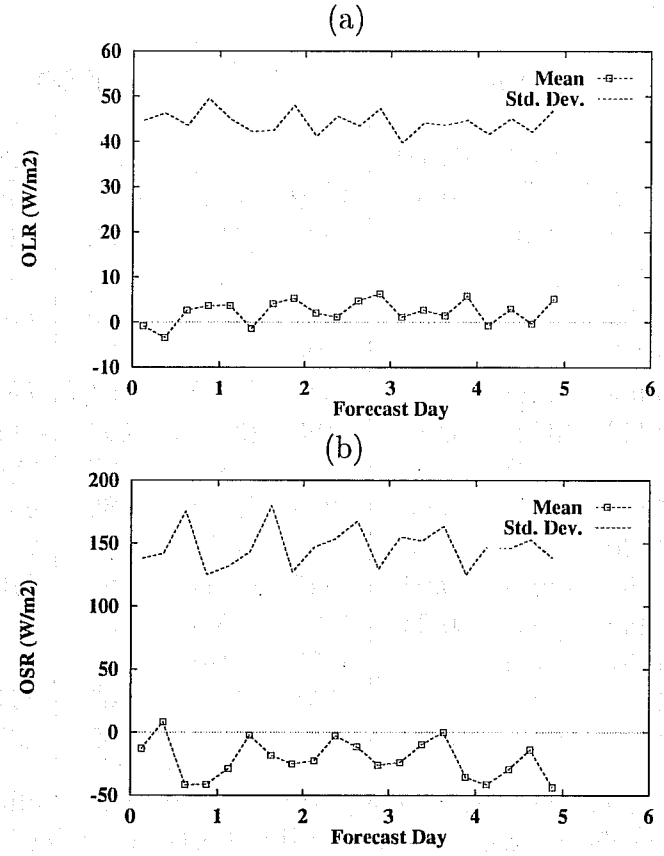

Figure 1: Comparison between the top-of-the-atmosphere radiation in the ECMWF 5-day forecast model and the corresponding CERES measurements: mean and standard deviation of the differences, in $W.m^{-2}$, for the period from the 1^{st} to the 21^{st} of July (21 cases). By convention, both the OLR and the OSR are set to be positive. (a) upward longwave. (b) upward shortwave.

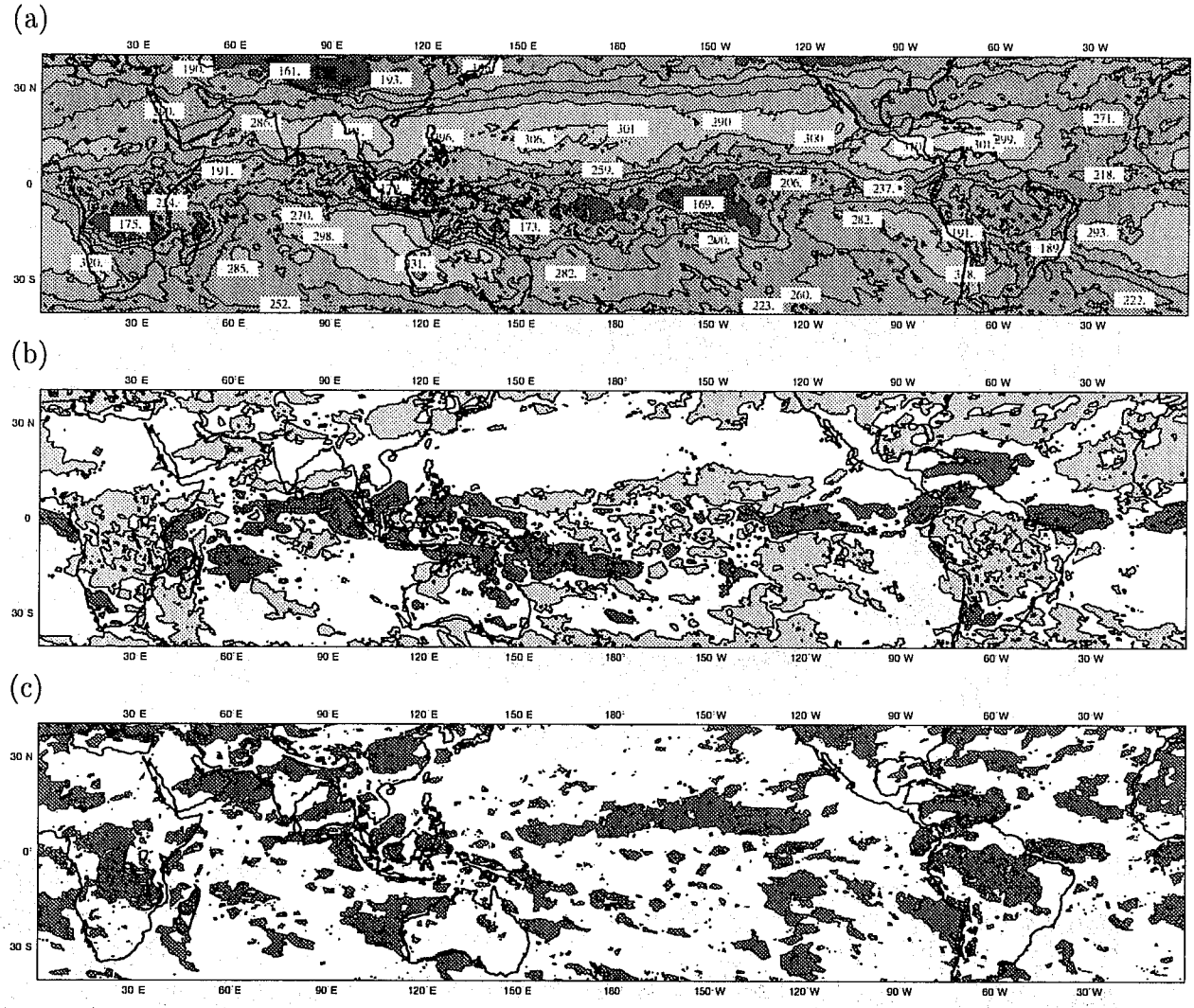

Figure 2: Comparison between the top-of-the-atmosphere longwave radiation in the ECMWF 6-hour forecast and the corresponding CERES measurements, in $W.m^{-2}$, for the period from the 1^{st} to the 21^{st} of January. (a) Mean CERES field. Contours every 20 $W.m^{-2}$; the main local extrema are indicated. (b) Mean differences (ECMWF - CERES). Contours every 20 $W.m^{-2}$; negative values less than -10 $W.m^{-2}$ are dark-shaded, positive values greater than 10 $W.m^{-2}$ are light-shaded. (c) Statistical significance of the differences shown in (b). Values greater than 0.95 are shaded.

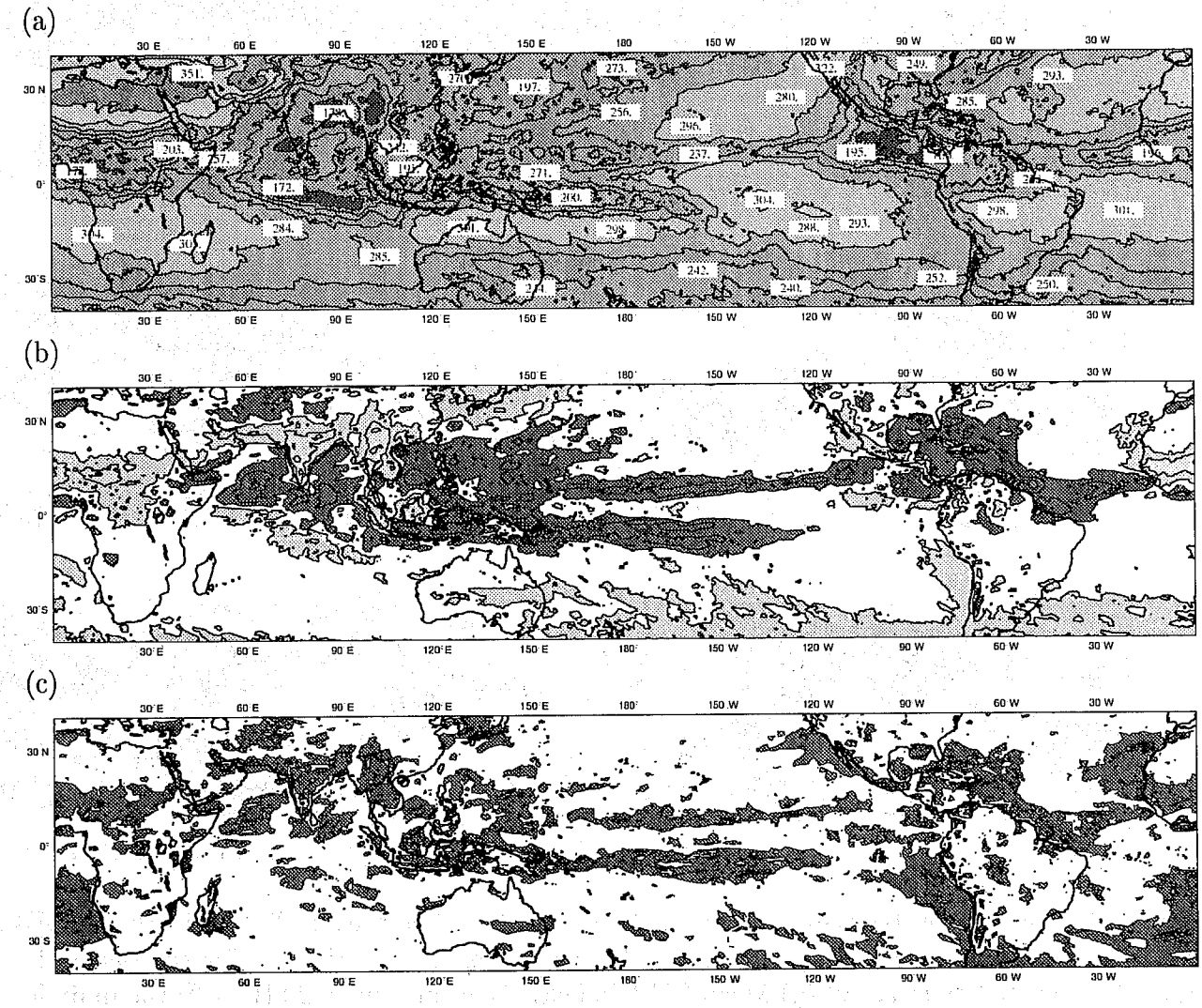

Figure 3: Same as previous for the period from the 1^{st} to the 21^{st} of July.

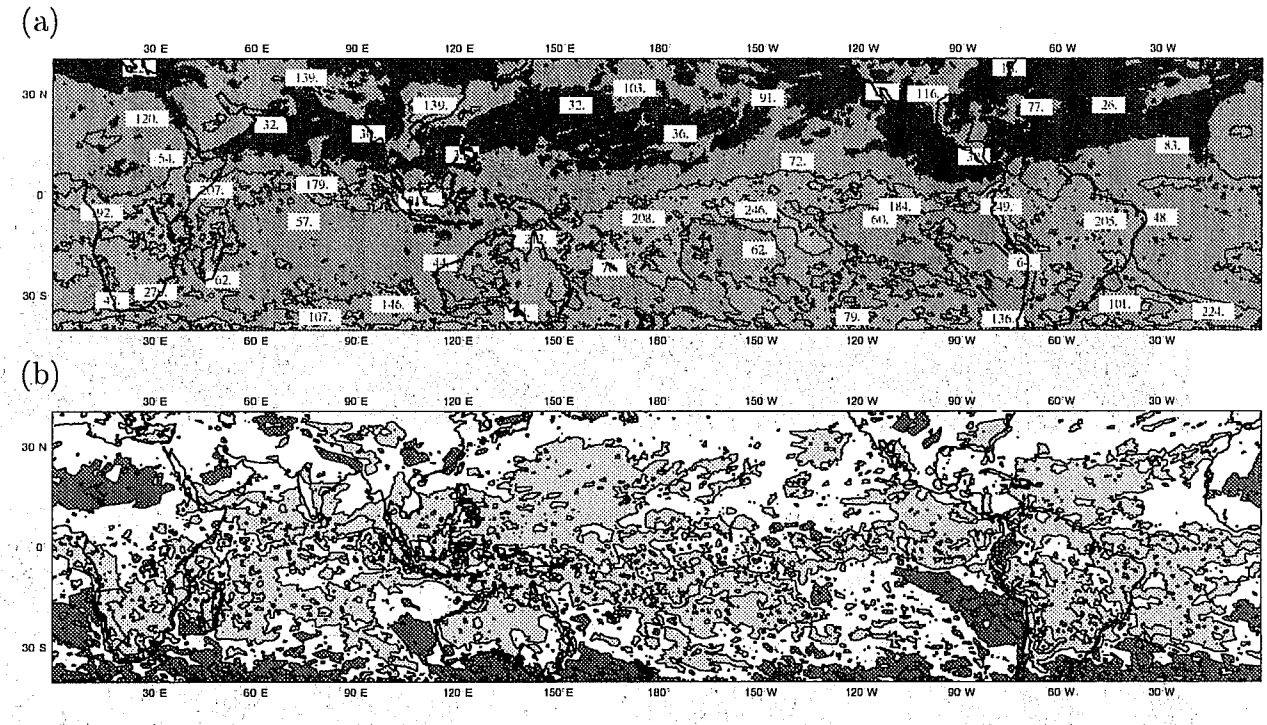

Figure 4: Comparison between the top-of-the-atmosphere shortwave radiation in the ECMWF 6-hour forecast and the corresponding CERES measurements, in $W.m^{-2}$, for the period from the 1^{st} to the 21^{st} of January. (a) Mean CERES field. Contours every 60 $W.m^{-2}$; the main local extrema are indicated. (b) Mean differences (ECMWF - CERES). Contours every 40 $W.m^{-2}$; negative values less than -20 $W.m^{-2}$ are dark-shaded, positive values greater than 20 $W.m^{-2}$ are light-shaded. Due both to the shortness of the period and to the shortwave diurnal cycle, no statistical significance test is performed.

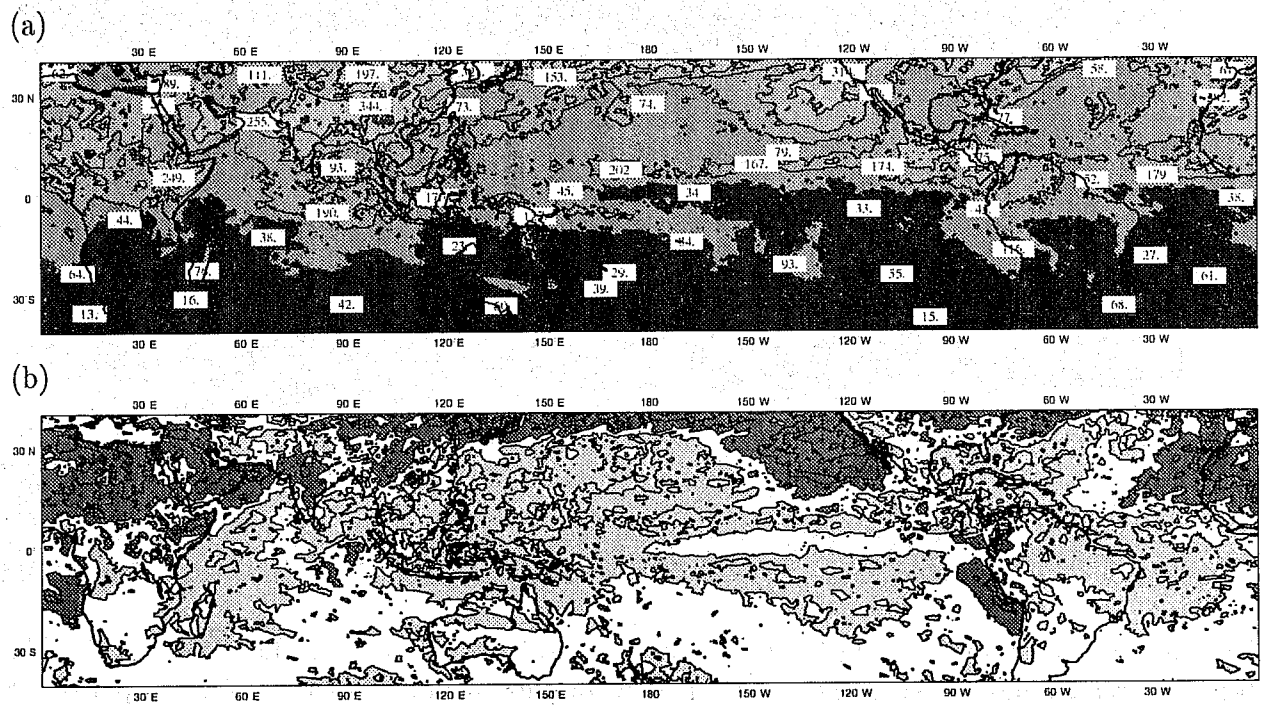

Figure 5: Same as previous, but for the upward shortwave radiation for the period from the 1^{st} to the 21^{st} of July. The minimum mean difference reaches -180 $W.m^{-2}$.

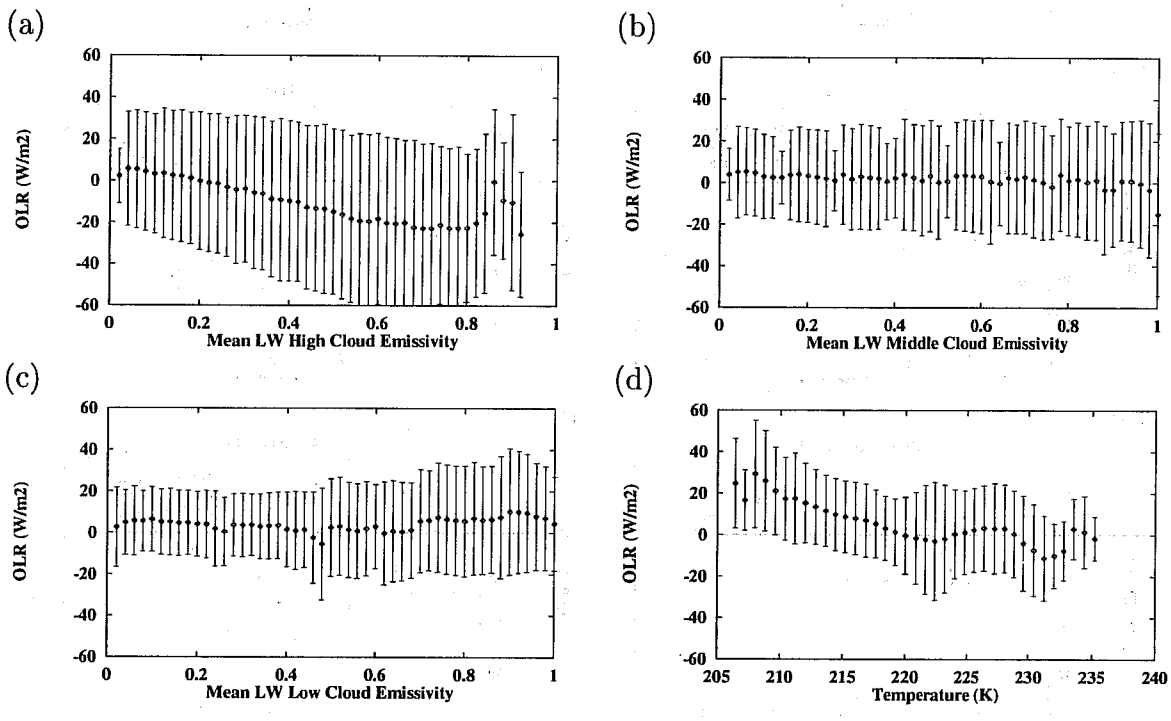

Figure 6: Difference between the top-of-the-atmosphere longwave radiation in the ECMWF 6-hour forecast and the corresponding CERES measurements (ECMWF - CERES, in $W.m^{-2}$), as a function of mean longwave cloud emissivity, for high (a), middle (b) and low (c) clouds, and as a function of the 200 hPa temperature (d). Cloud properties and temperature from the forecasts. Period from the 1^{st} to the 21^{st} of July. The squares and the vertical bars respectively represent the mean and the standard deviation after a 2-sigma elimination in each histogram class.

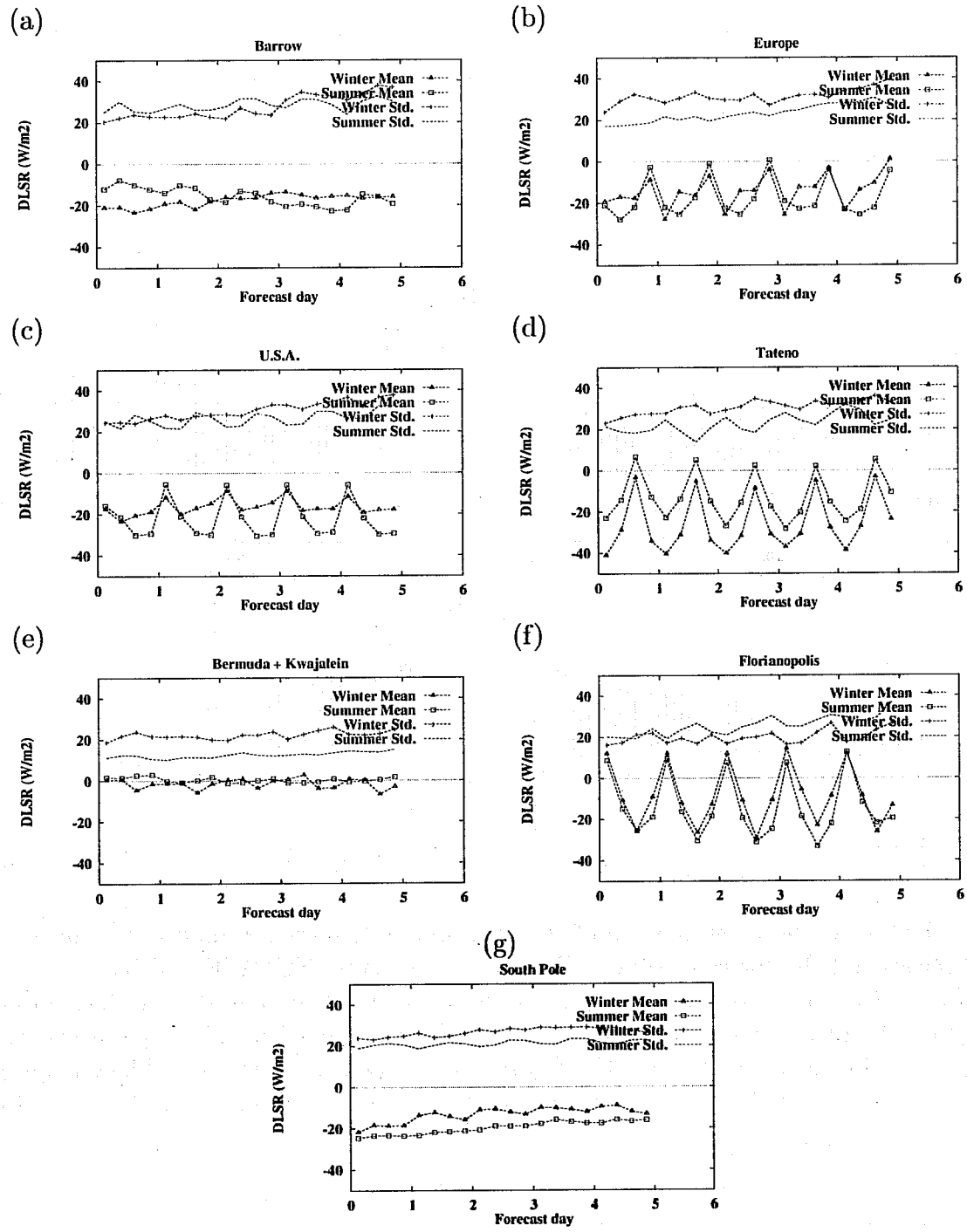

Figure 7: Comparison between the downward surface longwave radiation (DLSR) in the ECMWF 5-day forecast model and surface measurements: mean (ECMWF - observation) and standard deviation of the differences, in $W.m^{-2}$. The winter period corresponds to January and February 1998. The summer period corresponds to July and August 1998. The forecasts start at 12 UTC.

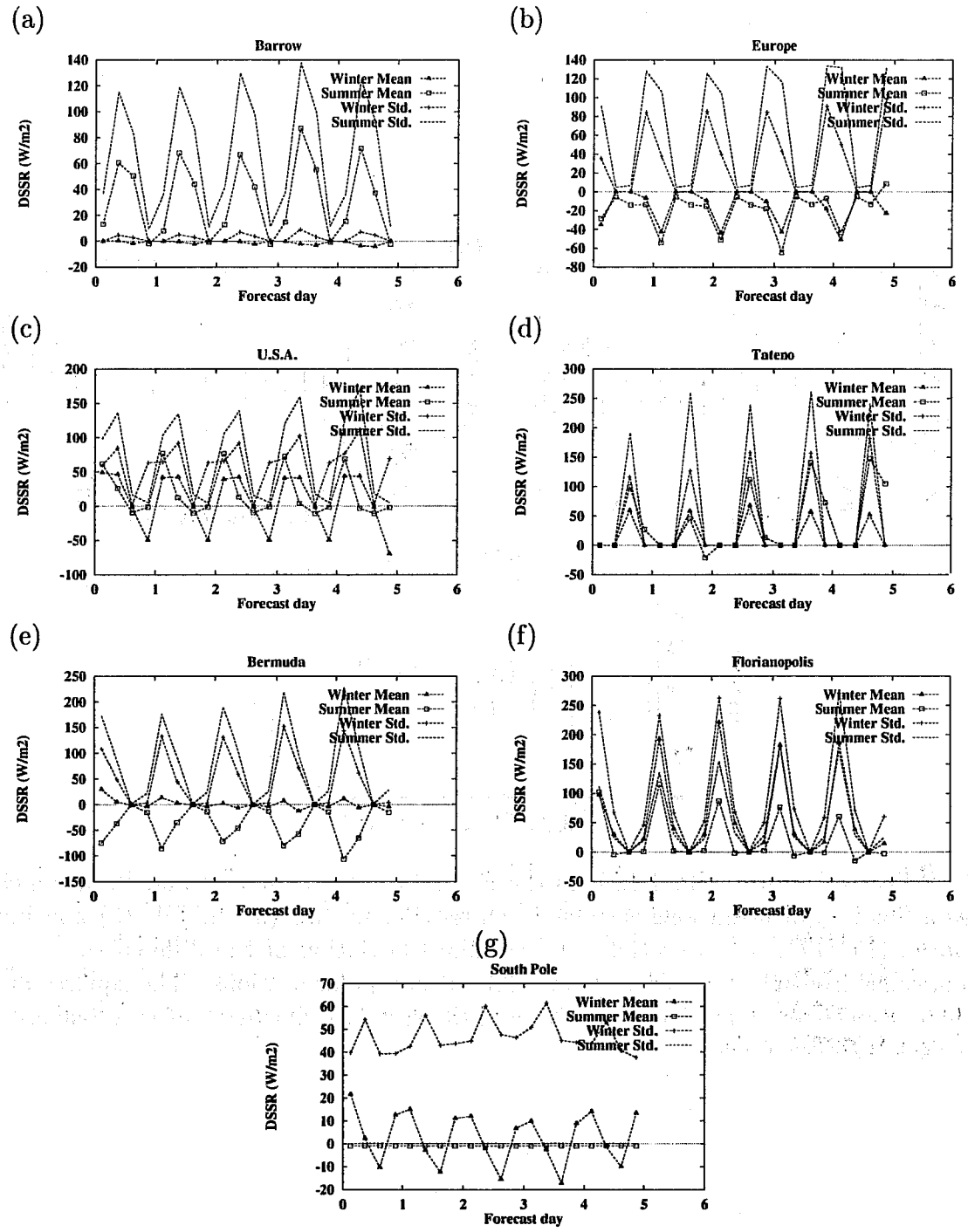

Figure 8: Same as previous, but for the shortwave.

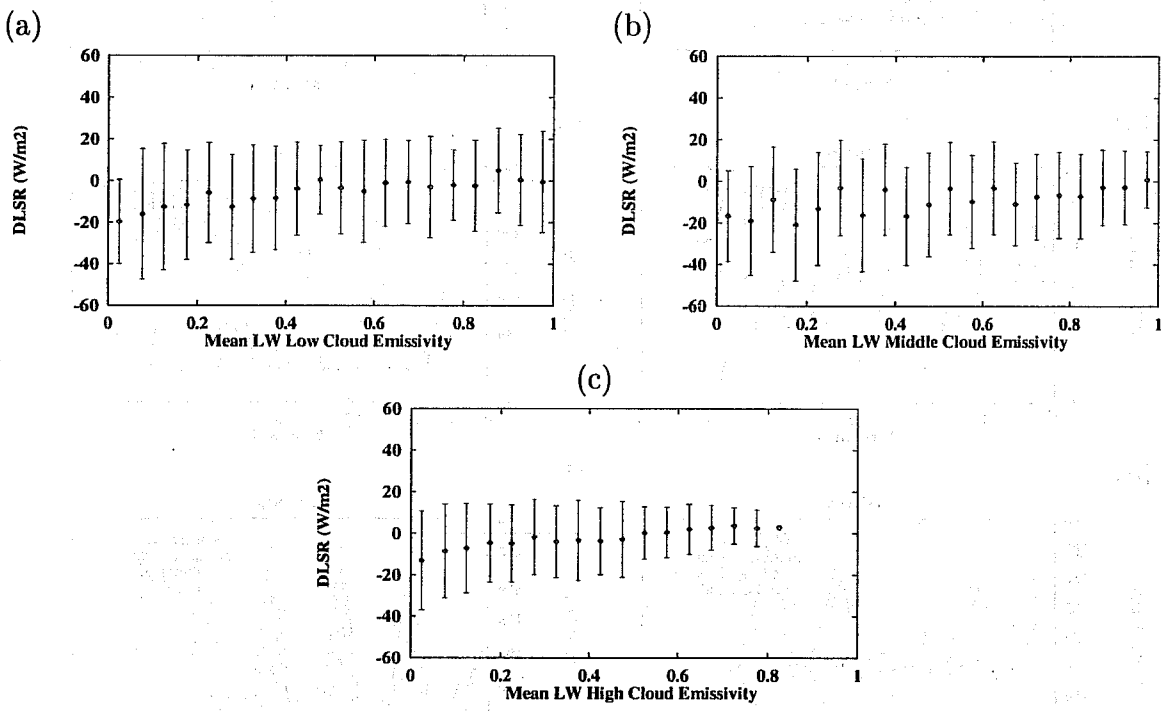

Figure 9: Difference between the DLSR in the ECMWF 6-hour forecast and surface measurements, as a function of mean longwave cloud emissivity, for low (a), middle (b) and high (c) clouds: mean (ECMWF - observation) and standard deviation of the differences, in $W.m^{-2}$. Cloud properties from the forecasts. Year 1998, all non-polar stations. The squares and the vertical bars respectively represent the mean and the standard deviation after a 2-sigma elimination in each histogram class.

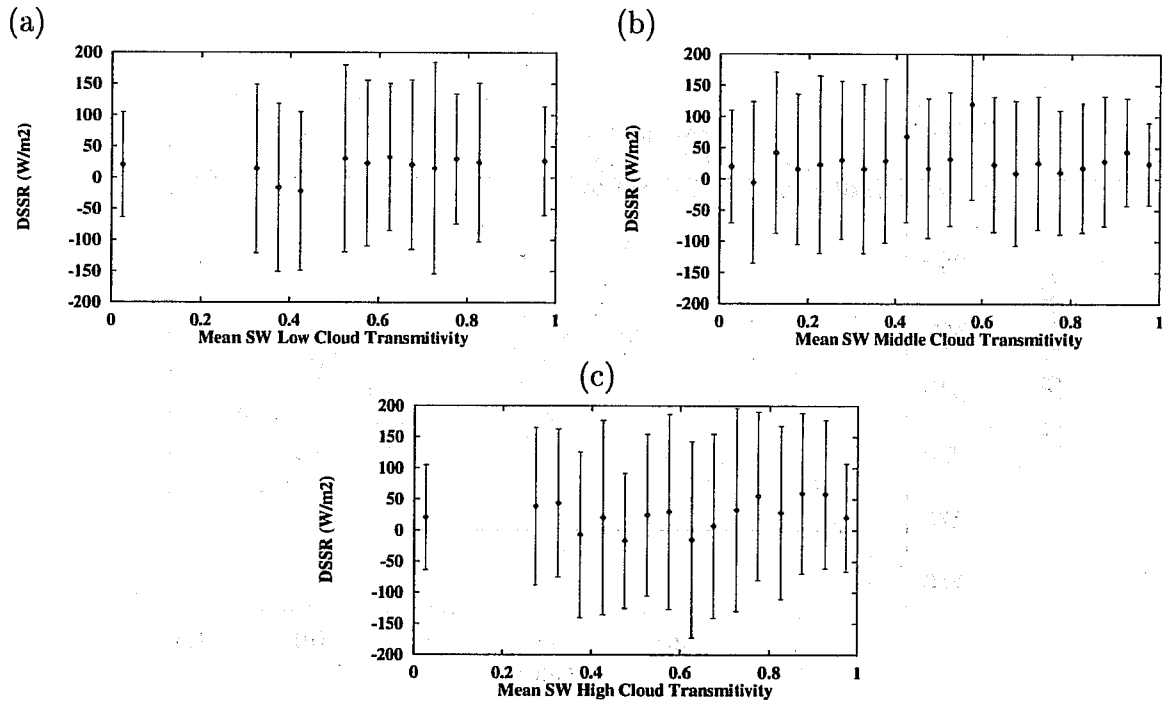

Figure 10: Difference between the DSSR in the ECMWF 6-hour forecast and surface measurements, as a function of mean shortwave cloud transmittivity in the 0.25-0.69 μm interval, for low (a), middle (b) and high (c) clouds: mean (ECMWF - observation) and standard deviation of the differences, in $W.m^{-2}$. Cloud properties from the forecasts. Year 1998, for local times between 9 GMT and 15 GMT. The squares and the vertical bars respectively represent the mean and the standard deviation after a 2-sigma elimination in each histogram class.

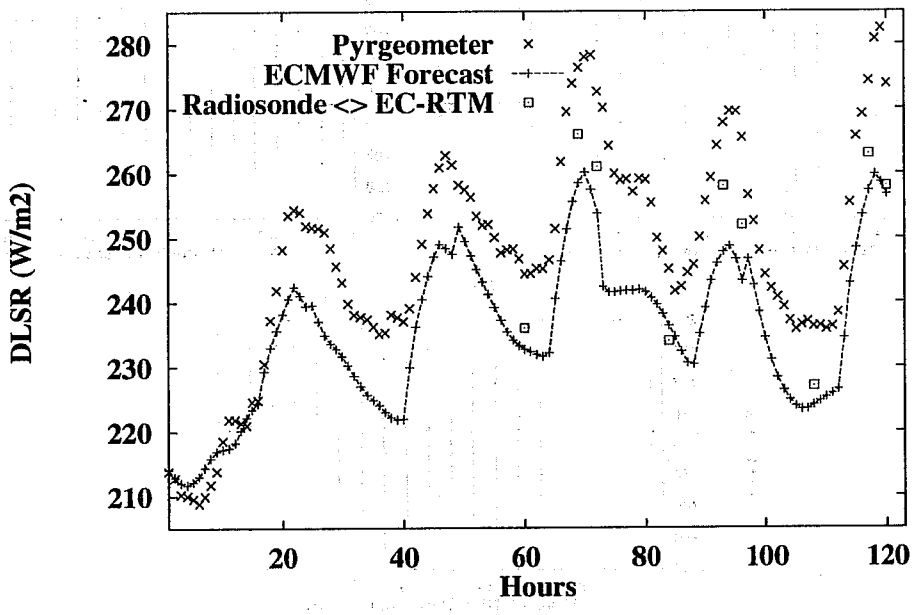

Figure 11: Comparison between the ECMWF forecasted DLSR, the pyrgeometer observation, and the radiosonde-derived DLSR using the ECMWF longwave radiative transfer model (EC-RTM). Billings site. Period from 13/12/97 to 17/12/97. The ECMWF variables are archived at every time step at Billings, but only 1-hour means are presented here.

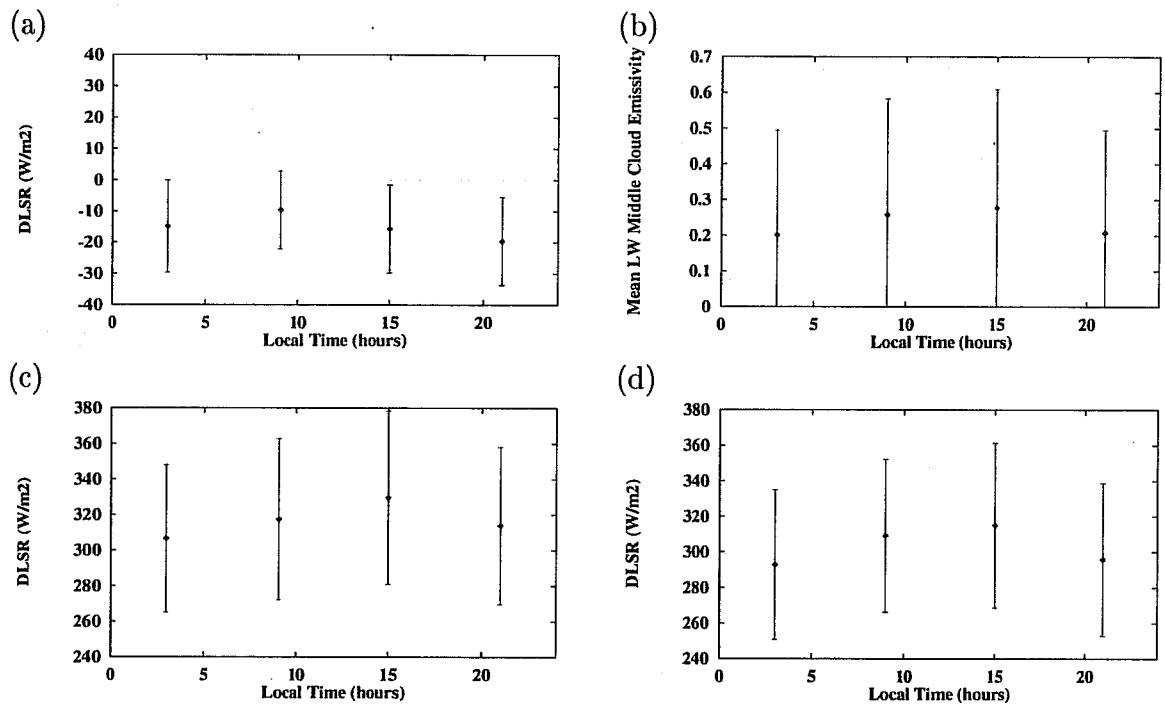

Figure 12: (a) Difference between the DLSR in the ECMWF 6-hour forecast and surface measurements at Carpentras, as a function of local time, in hours. (b) Mean longwave middle cloud emissivity (from the ECMWF 6-hour forecast) at Carpentras as a function of local time. (c) Observed downward longwave surface flux as a function of local time. (d) ECMWF 6-hour forecast downward longwave surface flux as a function of local time. Year 1998. Cloud properties from the forecasts. The squares and the vertical bars respectively represent the mean and the standard deviation after a 2-sigma elimination in each histogram class.